ELSEVIER

International Journal of Solids and Structures 41 (2004) 1625–1643

INTERNATIONAL JOURNAL OF SOLIDS and STRUCTURES

www.elsevier.com/locate/ijsolstr

Analytical solution for the cylindrical bending vibration of piezoelectric composite plates

Senthil S. Vel [a,*], R.C. Mewer [a], R.C. Batra [b]

[a] *Department of Mechanical Engineering, University of Maine, 5711 Boardman Hall, Room 214, Orono, ME 04469-5711, USA*
[b] *Department of Engineering Science and Mechanics, M/C 0219, Virginia Polytechnic Institute and State University, Blacksburg, VA 24061, USA*

Received 10 January 2003; received in revised form 2 October 2003

Abstract

An analytical solution for the cylindrical bending vibrations of linear piezoelectric laminated plates is obtained by extending the Stroh formalism to the generalized plane strain vibrations of piezoelectric materials. The laminated plate consists of homogeneous elastic or piezoelectric laminae of arbitrary thickness and width. Fourier basis functions for the mechanical displacements and electric potential that identically satisfy the equations of motion and the charge equation of electrostatics are used to solve boundary value problems via the superposition principle. The coefficients in the infinite series solution are determined from the boundary conditions at the edges and continuity conditions at the interfaces between laminae, which are satisfied in the sense of Fourier series. The formulation admits different boundary conditions at the edges of the laminated piezoelectric composite plate. Results for laminated elastic plates with either distributed or segmented piezoelectric actuators are presented for different sets of boundary conditions at the edges.

1. Introduction

When piezoelectric materials are integrated with structures, they are capable of altering the structure's response through sensing, actuation and control. Such structural systems, known as smart structures, are increasingly being used for self vibration suppression and health monitoring.

Initially piezoelectric actuators were used to control vibrations of beams (Bailey and Hubbard, 1985; Crawley and de Luis, 1987). The piezoelectric actuators used in beams are thin rectangular elements usually bonded to their outermost surfaces and are poled in the thickness direction. The application of an electric field in the thickness direction causes the actuator's lateral dimensions to change. The localized strains induced by the piezoelectric actuator in the host structure cause it to deform. In order to effectively integrate piezoelectric materials with structural systems, it is necessary to understand better the interaction between actuators and the base structure. Mechanical models have been developed by Crawley and de Luis

* Corresponding author. Tel.: +1-207-5812777; fax: +1-207-5812379.
E-mail address: senthil.vel@maine.edu (S.S. Vel).

0020-7683/$ - see front matter © 2003 Elsevier Ltd. All rights reserved.
doi:10.1016/j.ijsolstr.2003.10.012

(1987), Crawley and Anderson (1990) and others to analyze deformations and stresses in beams with surface-bonded piezoelectric actuators. Lee (1990), Wang and Rogers (1991), Batra and Ghosh (1995), Ghosh and Batra (1995), and Mitchell and Reddy (1995) have developed plate theories for composite laminates with embedded and/or surface mounted piezoelectric sensors and actuators. Numerous finite element studies have also been conducted (Allik and Hughes, 1970; Robbins and Reddy, 1991; Ha et al., 1992; Batra and Liang, 1997b; Batra and Geng, 2002).

Three-dimensional analytical solutions for the deformations and stresses in simply supported composite plates with piezoelectric layers have been given by Heyliger (1994, 1997), Heyliger and Brooks (1996), Heyliger and Saravanos (1995), Bisegna and Maceri (1996), Batra et al. (1996a), Batra and Liang (1997a), Lee and Jiang (1996) and Vel and Batra (2000a, 2001b), and for a functionally graded plate by Vel and Batra (2002). If one of the plate dimensions is very large as compared to the other two dimensions, then its deformations are generally regarded as being independent of the coordinate in that direction and the state of deformation is called cylindrical bending. Exact solutions for cylindrical bending of simply supported laminated plates were developed by Heyliger and Brooks (1996) and Vel and Batra (2001a), and for a functionally graded plate by Vel and Batra (2003), and for the cylindrical bending vibrations by Heyliger and Brooks (1995) and Yang et al. (1994). Brooks and Heyliger (1994) and Batra et al. (1996b) simulated a segmented piezoelectric actuator by applying an electric potential only over a part of a distributed piezoelectric actuator. Besides the edges being simply supported, only specific types of electric boundary conditions were considered and all layers were required to have the same width. However, simply supported edges are rarely encountered in practice and most smart structures have segmented piezoelectric patches with width much smaller than that of the host structure. Batra and Aimmanee (2003) have found frequencies missing in previous analytical solutions of free vibrations of simply supported homogeneous and laminated plates.

Vel and Batra (2000a) developed a three-dimensional quasi-static solution using the Stroh formalism for laminated piezoelectric rectangular plates subjected to arbitrary mechanical and electrical boundary conditions. Subsequently, they presented results for quasi-static cylindrical bending deformations of a laminated plate with segmented piezoelectric patches (Vel and Batra, 2000b). Here we analyze cylindrical bending vibrations of a laminated plate with embedded or surface mounted piezoelectric patches. Three-dimensional equations of linear piezoelectricity for generalized plane strain deformations are exactly satisfied by the chosen Fourier basis functions. Instead of assuming that the mechanical displacements and the electric field in the direction of the very large plate dimension vanish identically, the electric potential and the three components of the mechanical displacement are assumed to depend only on the two in-plane coordinates and time. The coefficients in the series solution are determined from boundary conditions at edges and continuity conditions at the interfaces between adjoining laminae. Computed natural frequencies, displacements and stresses for thick cantilever laminates containing either distributed or segmented actuators are found to compare very well with those obtained by the finite element method. We note that at the fixed end, all three components of mechanical displacement are set equal to zero.

2. Problem formulation

We use a rectangular Cartesian coordinate system, shown in Fig. 1, to describe the infinitesimal quasi-static deformations of a piezoelectric laminate occupying the region $[L^{(1)}, L^{(N_1+1)}] \times (-\infty, \infty) \times [H^{(1)}, H^{(N_3+1)}]$ in the unstressed reference configuration. Planes $x_3 = H^{(1)}, \ldots, H^{(n_3)}, \ldots, H^{(N_3+1)}$ describe the bottom bounding surface, the horizontal interfaces between adjoining laminae, and the top bounding surface. Planes $x_1 = L^{(1)}, \ldots, L^{(n_1)}, \ldots, L^{(N_1+1)}$ are respectively the left bounding surface, the vertical interfaces between adjoining laminae, and the right bounding surface. If the region $[L^{(n_1)}, L^{(n_1+1)}] \times (-\infty, \infty) \times [H^{(n_3)}, H^{(n_3+1)}]$ is occupied by material, we refer to it as the (n_1, n_3)th lamina.

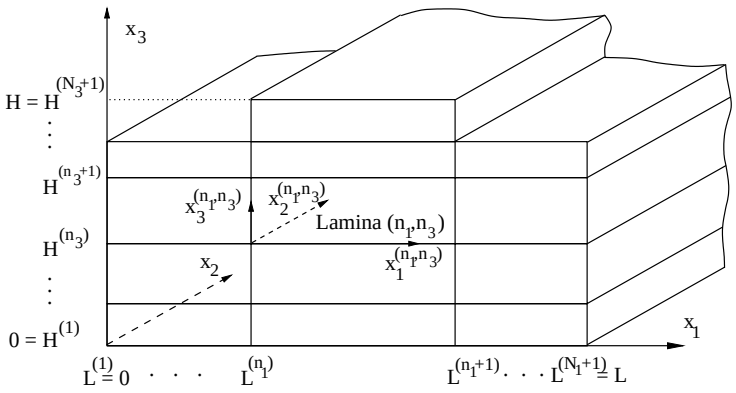

Fig. 1. Piezoelectric composite plate.

The equations of motion in the absence of body forces are

$$\sigma_{jm,m} = \rho \ddot{u}_j \quad (j, m = 1, 2, 3), \tag{1}$$

where σ_{jm} are components of the Cauchy stress tensor, ρ is the mass density and u_j are components of the mechanical displacement vector. A comma followed by index j indicates partial differentiation with respect to the present position x_j of a material particle, a superimposed dot indicates partial derivative with respect to time t, and a repeated index implies summation over the range of the index. The charge equation in the absence of free charges is

$$D_{m,m} = 0, \tag{2}$$

where D_m are components of the electric displacement vector.

The constitutive equations of a linear piezoelectric medium are (Tiersten, 1969)

$$\sigma_{jm} = C_{jmqr}\varepsilon_{qr} - e_{rjm}E_r, \qquad D_m = e_{mqr}\varepsilon_{qr} + \epsilon_{mr}E_r, \tag{3}$$

where C_{jmqr} is the elasticity tensor, ε_{qr} is the infinitesimal strain tensor, e_{rjm} are the piezoelectric coefficients that describe coupling between the mechanical deformation and electric field, E_r is the electric field and ϵ_{mr} is the electric permittivity tensor. The infinitesimal strain tensor and the electric field are related to the mechanical displacement u_q and the electric potential ϕ by

$$\varepsilon_{qr} = \frac{1}{2}(u_{q,r} + u_{r,q}), \qquad E_r = -\phi_{,r}. \tag{4}$$

The symmetry of the stress and the strain tensors and the existence of the stored energy function imply the following symmetries

$$C_{jmqr} = C_{mjqr} = C_{qrjm}, \qquad e_{rjm} = e_{rmj}, \qquad \epsilon_{mr} = \epsilon_{rm}. \tag{5}$$

Material constants are assumed to yield a positive stored energy density for every non-rigid deformation and/or non-zero electric field. That is,

$$C_{jmqr}\varepsilon_{jm}\varepsilon_{qr} > 0, \qquad \epsilon_{rm}E_rE_m > 0, \tag{6}$$

for every real non-zero ε_{jm} and E_r.

The boundary conditions on the top and bottom surfaces and the continuity conditions on the interface $x_3 = H^{(n_3)}$ of the (n_1, n_3)th lamina may be specified as follows:

(a) If the surface is not in contact with any other lamina, then boundary conditions are specified as

$$\mathbf{J}\begin{bmatrix}\mathbf{u}\\ \phi\end{bmatrix}+\widehat{\mathbf{J}}\begin{bmatrix}\boldsymbol{\sigma}_3\\ D_3\end{bmatrix}=\mathbf{f}(x_1)\cos\omega t \quad \text{on } x_3=H^{(n_3)}, \tag{7}$$

where ω is the forcing frequency and

$$(\boldsymbol{\sigma}_k)_i=\sigma_{ik}. \tag{8}$$

The function $\mathbf{f}(x_1)$ is prescribed and $\mathbf{J}$, $\widehat{\mathbf{J}}$ are 4×4 diagonal matrices with their elements functions of at most x_1. For most applications these diagonal matrices have entries either zero or one such that $\mathbf{J}+\widehat{\mathbf{J}}=\mathbf{I}$, where $\mathbf{I}$ is the 4×4 identity matrix. For example, if the surface is electroded and surface tractions are prescribed, then $\mathbf{J}=\mathrm{diag}[0,0,0,1]$ and $\widehat{\mathbf{J}}=\mathrm{diag}[1,1,1,0]$.

(b) If the surface is an interface between two laminae, then displacements, surface tractions, electric potential and the normal component of the electric displacement between them are taken to be continuous. That is

$$[\![\mathbf{u}]\!]=\mathbf{0}, \quad [\![\boldsymbol{\sigma}_3]\!]=\mathbf{0}, \quad [\![\phi]\!]=0, \quad [\![D_3]\!]=0 \quad \text{on } x_3=H^{(n_3)}. \tag{9}$$

Here $[\![\mathscr{F}]\!]$ denotes the jump in the value of $\mathscr{F}$ across an interface. Thus the adjoining laminae are presumed to be perfectly bonded together. We assume that the electrode is of negligible thickness.

(c) If the surface is an electroded interface, then the potential on this surface is a known function $f(x_1)$ while the normal component of the electric displacement need not be continuous across this interface, i.e.,

$$[\![\mathbf{u}]\!]=\mathbf{0}, \quad [\![\boldsymbol{\sigma}_3]\!]=\mathbf{0}, \quad \phi=f(x_1)\cos\omega t \quad \text{on } x_3=H^{(n_3)}. \tag{10}$$

The boundary/interface conditions may be similarly specified on the other three bounding surfaces $x_3=H^{(n_3+1)}$, $x_1=L^{(n_1)}$ and $x_1=L^{(n_1+1)}$. Note that the problem formulation allows for the length of a lamina to be less than the span L of the plate. Said differently, the region $H^{(n_3)}\leqslant x_3\leqslant H^{(n_3+1)}$, $0\leqslant x_1\leqslant L$ could be divided into several sections by vertical and horizontal planes with each section made of a different material.

We postulate that the displacement $\mathbf{u}$ and the electrical potential ϕ are functions of x_1, x_3 and time t; thus deformations of the laminate correspond to a generalized plane state of deformation. This assumption is reasonable since applied loads (mechanical and electrical) and material properties are independent of x_2 and the body is of infinite extent in the x_2 direction.

3. An analytical solution

We construct a local coordinate system $x_1^{(n_1,n_3)},x_2^{(n_1,n_3)},x_3^{(n_1,n_3)}$ with origin at the point $(L^{(n_1)},0,H^{(n_3)})$ in the global coordinate system and the local axes parallel to the global axes. The length and thickness of the (n_1,n_3)th lamina are denoted by $l^{(n_1,n_3)}=L^{(n_1+1)}-L^{(n_1)}$, $h^{(n_1,n_3)}=H^{(n_3+1)}-H^{(n_3)}$. In this section, we drop the superscripts (n_1,n_3) for convenience, it is understood that all material constants and unknowns belong to this lamina.

An analytical solution is obtained by extending the Stroh (Eshelby et al., 1953; Stroh, 1958; Ting, 1996) formalism to the analysis of steady state vibrations of piezoelectric composite plates. Fourier basis functions for the mechanical displacements and the electric potential, which identically satisfy the equations of motion (1) and charge equation (2), are used to compute the solution of the boundary value problem via the superposition principle. The coefficients in the series solution are determined from the boundary conditions (7) and continuity conditions (9) or (10) at the interfaces between adjoining laminae.

3.1. Sinusoidal basis functions in the x_1-direction

We assume the following form for the displacement vector and the electric potential

$$\begin{bmatrix} \mathbf{u} \\ \phi \end{bmatrix} = \mathbf{a}\exp(i\lambda z)\cos\omega t, \tag{11}$$

where $z = x_1 + px_3$, $i = \sqrt{-1}$, λ is a real number and the vector $\mathbf{a}$ and the scalar p will be determined from the equations of motion and the charge equation. The assumed mechanical displacement and the electric potential fields in (11) vary sinusoidally in the x_1-direction and λ determines its spatial period in that direction. Depending on whether p is complex or real, the assumed displacement and potential field (11) has either an exponential and/or sinusoidal variation in the x_3-direction. Substitution for $\mathbf{u}$ and ϕ from (11) into (4) and for ε and $\mathbf{E}$ into (3) gives the following expressions for components σ_{jm} of the stress tensor and D_m of the electric displacement vector:

$$\begin{aligned} \sigma_{jm} &= (C_{jmqr}a_q + e_{rjm}a_4)\lambda i(\delta_{r1} + p\delta_{r3})\exp(\lambda iz)\cos\omega t, \\ D_m &= (e_{mqr}a_q - \epsilon_{mr}a_4)\lambda i(\delta_{r1} + p\delta_{r3})\exp(\lambda iz)\cos\omega t, \end{aligned} \tag{12}$$

where δ_{rs} is the Kronecker delta. Substitution of (12) into the equation of motion (1) gives

$$\{C_{j1q1} + p(C_{j1q3} + C_{q1j3}) + p^2C_{j3q3}\}a_q + \{e_{11j} + p(e_{31j} + e_{13j}) + p^2e_{33j}\}a_4 = \frac{\rho\omega^2}{\lambda^2}a_j, \tag{13}$$

which can be written as

$$\{\widetilde{\mathbf{Q}} + p[\widetilde{\mathbf{R}} + \widetilde{\mathbf{R}}^{\mathrm{T}}] + p^2\widetilde{\mathbf{T}}\}\tilde{\mathbf{a}} + \{\mathbf{e}_{11} + p(\mathbf{e}_{31} + \mathbf{e}_{13}) + p^2\mathbf{e}_{33}\}a_4 = \frac{\rho\omega^2}{\lambda^2}\tilde{\mathbf{a}}, \tag{14}$$

where

$$\widetilde{Q}_{jq} = C_{j1q1}, \quad \widetilde{R}_{jq} = C_{j1q3}, \qquad \widetilde{T}_{jq} = C_{j3q3}, \quad (\mathbf{e}_{rm})_j = e_{rmj}, \qquad \tilde{\mathbf{a}} = \begin{bmatrix} a_1 \\ a_2 \\ a_3 \end{bmatrix}. \tag{15}$$

Substitution for D_m from (12) into the charge equation (2) gives

$$\{e_{11q} + p(e_{31q} + e_{13q}) + p^2e_{33q}\}a_q - \{\epsilon_{11} + p(\epsilon_{13} + \epsilon_{31}) + p^2\epsilon_{33}\}a_4 = 0, \tag{16}$$

which can be written as

$$\{\mathbf{e}_{11} + p(\mathbf{e}_{31} + \mathbf{e}_{13}) + p^2\mathbf{e}_{33}\}\tilde{\mathbf{a}} - \{\epsilon_{11} + p(\epsilon_{13} + \epsilon_{31}) + p^2\epsilon_{33}\}a_4 = 0. \tag{17}$$

The two Eqs. (14) and (17) can be combined to obtain (Ting, 1996)

$$\{\widehat{\mathbf{Q}} + p[\mathbf{R} + \mathbf{R}^{\mathrm{T}}] + p^2\mathbf{T}\}\mathbf{a} = \mathbf{0}, \tag{18}$$

where

$$\begin{aligned} &\widehat{\mathbf{Q}} = \mathbf{Q} - \frac{\rho\omega^2}{\lambda^2}\mathrm{diag}[1,1,1,0], \qquad \mathbf{Q} = \begin{bmatrix} \widetilde{\mathbf{Q}} & \mathbf{e}_{11} \\ \mathbf{e}_{11}^{\mathrm{T}} & -\epsilon_{11} \end{bmatrix}, \\ &\mathbf{R} = \begin{bmatrix} \widetilde{\mathbf{R}} & \mathbf{e}_{31} \\ \mathbf{e}_{13}^{\mathrm{T}} & -\epsilon_{13} \end{bmatrix}, \qquad \mathbf{T} = \begin{bmatrix} \widetilde{\mathbf{T}} & \mathbf{e}_{33} \\ \mathbf{e}_{33}^{\mathrm{T}} & -\epsilon_{33} \end{bmatrix}. \end{aligned} \tag{19}$$

Eq. (18) can be stated as the following algebraic eigenvalue problem (Ting, 1996)

$$\mathbf{N}\begin{bmatrix}\mathbf{a}\\ \mathbf{b}\end{bmatrix} = p\begin{bmatrix}\mathbf{a}\\ \mathbf{b}\end{bmatrix}, \tag{20}$$

where

$$\mathbf{N} = \begin{bmatrix} -\mathbf{T}^{-1}\mathbf{R}^{\mathrm{T}} & \mathbf{T}^{-1} \\ \mathbf{R}\mathbf{T}^{-1}\mathbf{R}^{\mathrm{T}} - \widehat{\mathbf{Q}} & -\mathbf{R}\mathbf{T}^{-1} \end{bmatrix},$$
$$\mathbf{b} = (\mathbf{R}^{\mathrm{T}} + p\mathbf{T})\mathbf{a} = -\frac{1}{p}(\widehat{\mathbf{Q}} + p\mathbf{R})\mathbf{a}. \tag{21}$$

The components (12) of the stress tensor and electric displacement vector can be written as

$$\begin{bmatrix}\boldsymbol{\sigma}_1\\ D_1\end{bmatrix} = \lambda i[\mathbf{Q} + p\mathbf{R}]\mathbf{a}\exp(\lambda i z)\cos\omega t,$$
$$\begin{bmatrix}\boldsymbol{\sigma}_3\\ D_3\end{bmatrix} = \lambda i[\mathbf{R}^{\mathrm{T}} + p\mathbf{T}]\mathbf{a}\exp(\lambda i z)\cos\omega t. \tag{22}$$

Since $\mathbf{N}$ is an 8×8 real matrix, there are eight eigensolutions $(p_\alpha, \mathbf{a}_\alpha)$, $\alpha = 1, 2, \ldots, 8$, to the algebraic eigenvalue problem (20); these eigensolutions depend upon values of the electromechanical parameters and the frequency ω. If p is a complex eigenvalue and $\mathbf{a}$ is the corresponding complex eigenvector, then the complex conjugates $\bar{p}$ and $\bar{\mathbf{a}}$ also form an eigensolution. Let there be 2κ complex and $8 - 2\kappa$ real eigenvalues. They are arranged as $p_1, \ldots, p_\kappa, p_{\kappa+1}, \ldots, p_{2\kappa}, p_{2\kappa+1}, \ldots, p_8$ such that

$$\mathrm{Im}(p_\alpha) > 0, \quad p_{\kappa+\alpha} = \bar{p}_\alpha, \quad \mathbf{a}_{\kappa+\alpha} = \bar{\mathbf{a}}_\alpha, \quad (\alpha = 1, \ldots, \kappa). \tag{23}$$

Mechanical displacements, electric potential, stresses and electric displacements vary sinusoidally in the x_1-direction on the surface $x_3^{(n_1,n_3)} = 0$. The basis function (11) constitutes one term of a Fourier series solution that will be used to satisfy the boundary conditions on $x_3^{(n_1,n_3)} = 0$. For complex p_α, the basis function decays exponentially in the x_3-direction due to the inequality in Eq. (23). The basis functions corresponding to real p_α vary sinusoidally in the x_3-direction.

In a similar manner, the following basis functions

$$\begin{bmatrix}\mathbf{u}\\ \phi\end{bmatrix} = \mathbf{a}\exp[\lambda i(ph - z)]\cos\omega t, \tag{24}$$

are used to satisfy the boundary conditions on the surface $x_3 = h$ of laminae (n_1, n_3). Substitution of (24) into the equation of motion (1) and the charge equation (2) also results in the eigenvalue problem (20) for p and $\mathbf{a}$. The corresponding components of the stress tensor and the electric displacement vector are

$$\begin{bmatrix}\boldsymbol{\sigma}_1\\ D_1\end{bmatrix} = -\lambda i[\mathbf{Q} + p\mathbf{R}]\mathbf{a}\exp[\lambda i(ph - z)]\cos\omega t,$$
$$\begin{bmatrix}\boldsymbol{\sigma}_3\\ D_3\end{bmatrix} = -\lambda i[\mathbf{R}^{\mathrm{T}} + p\mathbf{T}]\mathbf{a}\exp[\lambda i(ph - z)]\cos\omega t. \tag{25}$$

3.2. Sinusoidal basis functions in the x_3-direction

We assume the following form for the displacement vector and electric potential

$$\begin{bmatrix}\mathbf{u}\\ \phi\end{bmatrix} = \mathbf{c}\exp(\xi i z/q)\cos\omega t, \tag{26}$$

where ξ is a real number, $z = x_1 + qx_3$ and the vector $\mathbf{c}$ and the scalar q are unknowns. Note that $z/q = x_1/q + x_3$. The variation of the assumed mechanical displacement and electric field (26) in the x_3-direction is sinusoidal and ξ determines the wave length. Depending on whether q is complex or real, the assumed displacement and potential fields vary either exponentially and/or sinusoidally in the x_1-direction. From Eqs. (26), (4) and (3) we obtain

$$\begin{aligned} \sigma_{jm} &= \frac{\xi i}{q}(C_{jmqr}c_q + e_{rjm}c_4)(\delta_{r1} + q\delta_{r3})\exp(\xi i z/q)\cos\omega t, \\ D_m &= \frac{\xi i}{q}(e_{mqr}c_q - \epsilon_{mr}c_4)(\delta_{r1} + q\delta_{r3})\exp(\xi i z/q)\cos\omega t, \end{aligned} \tag{27}$$

which we write as

$$\begin{aligned} \begin{bmatrix} \boldsymbol{\sigma}_1 \\ D_1 \end{bmatrix} &= \frac{\xi i}{q}[\mathbf{Q} + q\mathbf{R}]\mathbf{c}\exp(\xi i z/q)\cos\omega t, \\ \begin{bmatrix} \boldsymbol{\sigma}_3 \\ D_3 \end{bmatrix} &= \frac{\xi i}{q}[\mathbf{R}^{\mathrm{T}} + q\mathbf{T}]\mathbf{c}\exp(\xi i z/q)\cos\omega t, \end{aligned} \tag{28}$$

where $\mathbf{Q}$, $\mathbf{R}$ and $\mathbf{T}$ are defined in (19). Substitution of (26) and (27) into (1) and (2) gives

$$\{\mathbf{Q} + q[\mathbf{R} + \mathbf{R}^{\mathrm{T}}] + q^2\widehat{\mathbf{T}}\}\mathbf{c} = \mathbf{0}, \tag{29}$$

where

$$\widehat{\mathbf{T}} = \mathbf{T} - \frac{\rho\omega^2}{\xi^2}\mathrm{diag}[1,1,1,0].$$

Eq. (29) constitutes the following algebraic eigenvalue problem:

$$\mathbf{N}\begin{bmatrix} \mathbf{c} \\ \mathbf{d} \end{bmatrix} = q\begin{bmatrix} \mathbf{c} \\ \mathbf{d} \end{bmatrix}, \tag{30}$$

where

$$\begin{aligned} \mathbf{N} &= \begin{bmatrix} -\widehat{\mathbf{T}}^{-1}\mathbf{R}^{\mathrm{T}} & \widehat{\mathbf{T}}^{-1} \\ \mathbf{R}\widehat{\mathbf{T}}^{-1}\mathbf{R}^{\mathrm{T}} - \mathbf{Q} & -\mathbf{R}\widehat{\mathbf{T}}^{-1} \end{bmatrix}, \\ \mathbf{d} &= (\mathbf{R}^{\mathrm{T}} + q\widehat{\mathbf{T}})\mathbf{c} = -\frac{1}{q}(\mathbf{Q} + q\mathbf{R})\mathbf{c}. \end{aligned} \tag{31}$$

Eigenvalues of (30) are arranged in the same was as those of (20). The basis function (26) makes one term of a Fourier series solution used to satisfy boundary conditions on the surface $x_1 = 0$ of the (n_1, n_3)th lamina. Similarly, the following basis function (32) is used to satisfy the boundary conditions on the surface $x_1 = l$ of the lamina (n_1, n_3)

$$\begin{bmatrix} \mathbf{u} \\ \phi \end{bmatrix} = \mathbf{c}\exp[\xi i(l - z)/q]\cos\omega t. \tag{32}$$

The stresses and the electric displacements corresponding to the basis function (32) are

$$\begin{aligned} \begin{bmatrix} \boldsymbol{\sigma}_1 \\ D_1 \end{bmatrix} &= -\frac{\xi i}{q}[\mathbf{Q} + q\mathbf{R}]\mathbf{c}\exp[\xi i(l - z)/q]\cos\omega t, \\ \begin{bmatrix} \boldsymbol{\sigma}_3 \\ D_3 \end{bmatrix} &= -\frac{\xi i}{q}\left[\mathbf{R}^{\mathrm{T}} + q\mathbf{T}\right]\mathbf{c}\exp[\xi i(l - z)/q]\cos\omega t. \end{aligned} \tag{33}$$

3.3. Superposition of basis functions

For distinct p_α, we can superimpose solutions of the form (11), (24), (26) and (32) to obtain the following mechanical displacement and electric potential fields:

$$\begin{bmatrix}\mathbf{u}\\ \phi\end{bmatrix} = \left\{\sum_{k=0}^{\infty}\sum_{\alpha=1}^{8}\{r_\alpha^{(k)}\exp(\lambda^{(k)}iz_\alpha^{(k)}) + s_\alpha^{(k)}\exp[\lambda^{(k)}i(p_\alpha^{(k)}h - z_\alpha^{(k)})]\}\mathbf{a}_\alpha^{(k)}\right.$$
$$\left. + \sum_{m=0}^{\infty}\sum_{\alpha=1}^{8}\left\{v_\alpha^{(m)}\exp\left(\frac{\xi_\alpha^{(m)}i\tilde{z}_\alpha^{(m)}}{q_\alpha^{(m)}}\right) + w_\alpha^{(m)}\exp\left[\frac{\xi_\alpha^{(m)}i(l-\tilde{z}_\alpha^{(m)})}{q_\alpha^{(m)}}\right]\right\}\mathbf{c}_\alpha^{(m)}\right\}\cos\omega t, \tag{34}$$

where

$$\lambda^{(k)} = \begin{cases}\frac{k_0\pi i}{l} & \text{if } k=0\\ \frac{k\pi i}{l} & \text{if } k\geqslant 1\end{cases}, \qquad \xi_\alpha^{(m)} = \begin{cases}-\frac{m_0\pi i}{q_\alpha h} & \text{if } m=0\\ -\frac{m\pi i}{q_\alpha h} & \text{if } m\geqslant 1\end{cases}, \tag{35}$$

$z_\alpha^{(k)} = x_1 + p_\alpha^{(k)}x_3$, $\tilde{z}_\alpha^{(m)} = x_1 + q_\alpha^{(m)}x_3$ and $(k_0, m_0) \in (0,1)$. The basis functions corresponding to $\lambda^{(0)}$ and $\xi_\alpha^{(0)}$ play the role of the constant term in the Fourier series expansion. The constants $r_\alpha^{(k)}$, $s_\alpha^{(k)}$, $v_\alpha^{(m)}$ and $w_\alpha^{(m)}$ are the Fourier coefficients in the series solution. In order to obtain real valued displacements and potentials, we assume that the coefficients r_α, s_α, v_α and w_α are complex for $\alpha \leqslant 2\kappa$ and real for $\alpha > 2\kappa$, such that $r_{\kappa+\alpha} = \bar{r}_\alpha$, $s_{\kappa+\alpha} = \bar{s}_\alpha$, $v_{\kappa+\alpha} = \bar{v}_\alpha$, $w_{\kappa+\alpha} = \bar{w}_\alpha$ for $\alpha = 1, \ldots, \kappa$.

The components of the stress tensor and the electric displacement vector corresponding to the series solution (34), obtained by superposition of Eqs. (22), (25), (28) and (33), are

$$\begin{bmatrix}\boldsymbol{\sigma}_1\\ D_1\end{bmatrix} = \left\{\sum_{k=0}^{\infty}\sum_{\alpha=1}^{8}\lambda^{(k)}i\{r_\alpha^{(k)}\exp(\lambda^{(k)}iz_\alpha^{(k)}) - s_\alpha^{(k)}\exp[\lambda^{(k)}i(p_\alpha^{(k)}h - z_\alpha^{(k)})]\}[\mathbf{Q} + p_\alpha^{(k)}\mathbf{R}]\mathbf{a}_\alpha^{(k)}\right.$$
$$\left. + \sum_{m=0}^{\infty}\sum_{\alpha=1}^{8}\frac{\xi_\alpha^{(m)}i}{q_\alpha^{(m)}}\left\{v_\alpha^{(m)}\exp\left(\frac{\xi_\alpha^{(m)}i\tilde{z}_\alpha^{(m)}}{q_\alpha^{(m)}}\right) - w_\alpha^{(m)}\exp\left[\frac{\xi_\alpha^{(m)}i(l-\tilde{z}_\alpha^{(m)})}{q_\alpha^{(m)}}\right]\right\}[\mathbf{Q} + q_\alpha^{(m)}\mathbf{R}]\mathbf{c}_\alpha^{(m)}\right\}\cos\omega t, \tag{36}$$

$$\begin{bmatrix}\boldsymbol{\sigma}_3\\ D_3\end{bmatrix} = \left\{\sum_{k=0}^{\infty}\sum_{\alpha=1}^{8}\lambda^{(k)}i\{r_\alpha^{(k)}\exp(\lambda^{(k)}iz_\alpha^{(k)}) - s_\alpha^{(k)}\exp[\lambda^{(k)}i(p_\alpha^{(k)}h - z_\alpha^{(k)})]\}[\mathbf{R}^{\mathrm{T}} + p_\alpha^{(k)}\mathbf{T}]\mathbf{a}_\alpha^{(k)}\right.$$
$$\left. + \sum_{m=0}^{\infty}\sum_{\alpha=1}^{8}\frac{\xi_\alpha^{(m)}i}{q_\alpha^{(m)}}\left\{v_\alpha^{(m)}\exp\left(\frac{\xi_\alpha^{(m)}i\tilde{z}_\alpha^{(m)}}{q_\alpha^{(m)}}\right) - w_\alpha^{(m)}\exp\left[\frac{\xi_\alpha^{(m)}i(l-\tilde{z}_\alpha^{(m)})}{q_\alpha^{(m)}}\right]\right\}[\mathbf{R}^{\mathrm{T}} + q_\alpha^{(m)}\mathbf{T}]\mathbf{c}_\alpha^{(m)}\right\}\cos\omega t. \tag{37}$$

4. Satisfaction of boundary and interface conditions

The unknowns $r_\alpha^{(k)}$, $s_\alpha^{(k)}$, $v_\alpha^{(m)}$, $w_\alpha^{(m)}$ for each lamina (n_1, n_3) are determined by imposing the interface continuity conditions and boundary conditions on all surfaces of the laminate by the classical Fourier series

method. For example, let boundary conditions (7) be specified on the surface $x_3^{(1,1)} = 0$ of lamina $(1,1)$. We multiply (7) by $\exp(j\pi i x_1^{(1,1)}/l^{(1,1)})$ and integrate with respect to $x_1^{(1,1)}$ from $-l^{(1,1)}$ to $l^{(1,1)}$ to obtain

$$\int_{-l^{(1,1)}}^{l^{(1,1)}} \left\{ \mathbf{J}^{(1,1)} \begin{bmatrix} \mathbf{u} \\ \phi \end{bmatrix}^{(1,1)} + \widehat{\mathbf{J}}^{(1,1)} \begin{bmatrix} \boldsymbol{\sigma}_3 \\ D_3 \end{bmatrix}^{(1,1)} - \mathbf{f}^{(1,1)}(x_1^{(1,1)}) \right\} \exp\left(j \frac{\pi i x_1^{(1,1)}}{l^{(1,1)}} \right) \mathrm{d}x_1^{(1,1)} = \mathbf{0}, \tag{38}$$

on $x_3^{(1,1)} = 0$ for $j = 0, 1, 2, \ldots$ In Eq. (38) the functions multiplying the coefficients $r_\alpha^{(k)}$ and $s_\alpha^{(k)}$ $(k \neq 0)$ have a sinusoidal variation in the x_1 direction and are extended over the interval $(-l^{(1,1)}, 0)$ without modification since they form the basis functions on this surface. The functions multiplying $v_\alpha^{(m)}$ and $w_\alpha^{(m)}$ have an exponential or sinusoidal variation in the x_1 direction; these are extended as even functions over the interval $(-l^{(1,1)}, 0)$. The functions multiplying $r_\alpha^{(0)}$, $s_\alpha^{(0)}$ are also extended as even functions since they play the role of the constant term in the Fourier series expansion. The known function $\mathbf{f}^{(1,1)}(x_1^{(1,1)})$ is extended in a suitable manner. If the surface $x_3^{(1,1)} = 0$ is an interface between two adjoining laminae then the conditions (9) or (10) are enforced instead of (7). Thus, upon imposing the boundary/interface conditions on all four bounding surfaces of every lamina in the laminated plate, we obtain an infinite system of linear algebraic equations for the infinitely many unknown coefficients. A general theory for the solution of an infinite set of algebraic equations does not exist. However, reasonably accurate results may be obtained by truncating the series with summation indices k and m in (34) to $K^{(n_1,n_3)}$ and $M^{(n_1,n_3)}$ terms respectively for the (n_1, n_3)th lamina. In general, we try to maintain approximately the same wave length of the largest harmonic on all the bounding surfaces of the lamina by choosing $K^{(n_1,n_3)} = \mathrm{Ceil}(Kl^{(n_1,n_3)}/L)$ and $M^{(n_1,n_3)} = \mathrm{Ceil}(Kh^{(n_1,n_3)}/L)$, where $\mathrm{Ceil}(y)$ equals the smallest integer greater than or equal to y. Thus the total number of unknowns will depend solely on the choice of integer K. Once the unknown coefficients have been evaluated by solving the truncated system of linear equations, the displacements and stresses in each lamina are obtained from (34), (36) and (37).

5. Results and discussion

A piezoelectric composite structure has a series of natural frequencies that can be arranged in ascending order as ω_j, $j = 1, 2, 3, \ldots$. These are determined by applying a potential to the piezoelectric actuator and plotting the vertical or axial component of the displacement for a specific point in the plate as a function of the forcing frequency. The displacement becomes large at certain discrete values of the forcing frequency, which signifies the resonance phenomenon.

5.1. Validation of the approach

The solution procedure and the program developed for numerical computations was validated by comparing the natural frequencies with those given by Heyliger and Brooks (1995) for the cylindrical bending vibration of a simply supported monolithic piezoelectric plate of length $L = 0.04$ m and thickness $H = 0.01$ m. The mechanical boundary conditions at the edges $x_1 = 0$ and L are specified as $u_3 = 0$, $\sigma_{11} = \sigma_{12} = 0$. The edges, and the bottom surfaces of the plate are electrically grounded to zero potential. Natural frequencies corresponding to the first axial mode of vibration are tabulated by Heyliger and Brooks (1995). A sinusoidal potential $\phi(x_1, H) = \phi_0 \sin(\pi x_1/L)\cos\omega t$ is applied to the top surface to excite various thickness modes corresponding to the first axial mode of vibration. The plate is made of PZT-4 whose non-zero material constants are given in Table 1. The axial displacement $u_1(0,0)$ is plotted as a function of the normalized forcing frequency $\bar{\omega}$ in Fig. 2, where $\bar{\omega} = \omega(L^2/H)\sqrt{\rho_0/C_0}$, $\rho_0 = 7600$ kg/m^3 and $C_0 = 138.499$ GPa. The axial displacement becomes large at $\bar{\omega} = 2.2603$, 10.087, 24.088, 41.663 and 49.511, which are natural frequencies of the plate. It should be noted that we will obtain the same set of

Table 1
Non-vanishing material properties of the graphite–epoxy, the PZT-4 and the PZT-5A materials poled in the x_3 direction

Material property	Graphite/epoxy	PZT-4	PZT-5A
C_{1111} (GPa)	183.443	138.499	99.201
C_{2222} (GPa)	11.662	138.499	99.201
C_{3333} (GPa)	11.662	114.745	86.856
C_{1122} (GPa)	4.363	77.371	54.016
C_{1133} (GPa)	4.363	73.643	50.778
C_{2233} (GPa)	3.918	73.643	50.778
C_{2323} (GPa)	2.870	25.6	21.100
C_{3131} (GPa)	7.170	25.6	21.100
C_{1212} (GPa)	7.170	30.6	22.593
e_{311} ($\mathrm{C\,m^{-2}}$)	0	−5.2	−7.209
e_{322} ($\mathrm{C\,m^{-2}}$)	0	−5.2	−7.209
e_{333} ($\mathrm{C\,m^{-2}}$)	0	15.08	15.118
e_{223} ($\mathrm{C\,m^{-2}}$)	0	12.72	12.322
e_{113} ($\mathrm{C\,m^{-2}}$)	0	12.72	12.322
ϵ_{11} (10^{-8} F/m)	1.53	1.306	1.53
ϵ_{22} (10^{-8} F/m)	1.53	1.306	1.53
ϵ_{33} (10^{-8} F/m)	1.53	1.1151	1.50
ρ ($\mathrm{kg/m^3}$)	1590	7600	7750

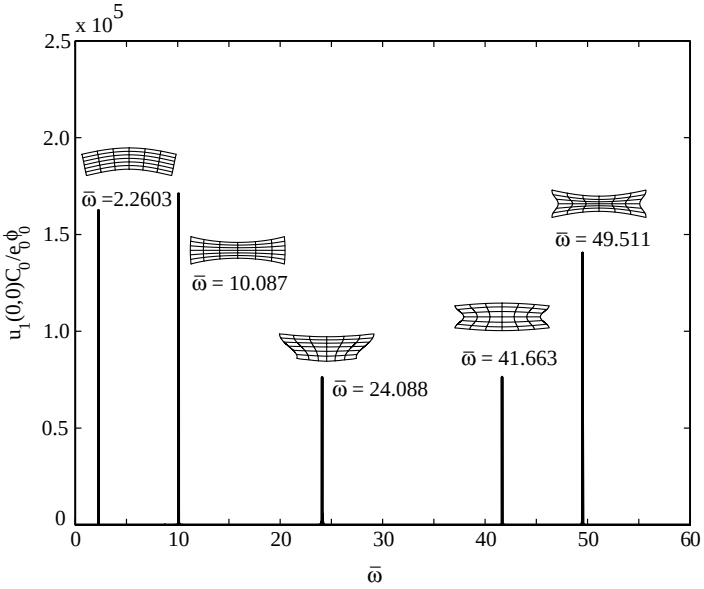

Fig. 2. First five normalized natural frequencies and mode shapes corresponding to the first axial mode of vibration for a thick simply supported PZT-4 plate.

natural frequencies if we plot the transverse displacement $u_3(L/2, 0)$ as a function of the forcing frequency ω except for the in-plane distortional modes for which the transverse displacement identically vanishes (e.g., see Batra and Aimmanee, 2003). The mode shapes corresponding to the natural frequencies are shown next

Table 2
Normalized natural frequencies $\bar{\omega}$ of a simply supported thick piezoelectric plate ($L/H = 4$)

Thickness mode	Present analysis	Heyliger and Brooks (1995)	Finite element analysis
1	2.2603	2.2606	2.2602
2	10.087	10.082	10.087
3	24.088	24.086	24.085
4	41.663	41.700	41.663
5	49.511	49.616	49.511

Table 3
Convergence study for the graphite/epoxy-PZT5A cantilever composite laminate ($L/H = 5$)

K	$\frac{\omega_1 L^2}{H}\sqrt{\frac{\rho_0}{C_0}}$	$\frac{u_3(\frac{L}{2},\frac{H}{2})}{u_3(L,\frac{H}{2})}$	$\frac{u_1(\frac{L}{2},H)}{u_3(L,\frac{H}{2})}$	$\frac{10^5\phi(\frac{L}{2},\frac{3H}{4})e_0}{C_0 u_3(L,\frac{H}{2})}$	$\frac{10\sigma_{11}(\frac{L}{4},0)L}{C_0 u_3(L,\frac{H}{2})}$	$\frac{10\sigma_{13}(\frac{L}{4},\frac{3H}{4})L}{C_0 u_3(L,\frac{H}{2})}$
50	1.1164	0.4034	−0.1470	8.279	2.747	0.2416
100	1.1149	0.4031	−0.1471	8.345	2.746	0.2409
150	1.1146	0.4032	−0.1471	8.362	2.743	0.2408
200	1.1145	0.4032	−0.1471	8.368	2.744	0.2408
250	1.1144	0.4032	−0.1472	8.371	2.746	0.2408
300	1.1144	0.4032	−0.1472	8.374	2.747	0.2408
350	1.1144	0.4032	−0.1472	8.375	2.746	0.2408
400	1.1144	0.4032	−0.1472	8.375	2.746	0.2408

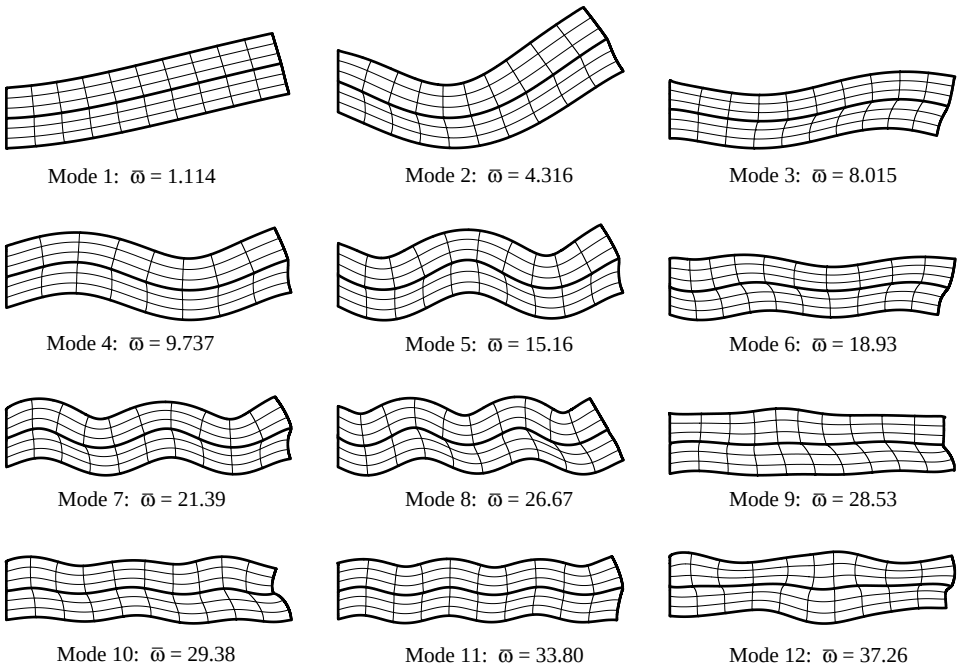

Fig. 3. First 12 normalized natural frequencies and mode shapes for the cantilever graphite/epoxy-PZT5A composite plate.

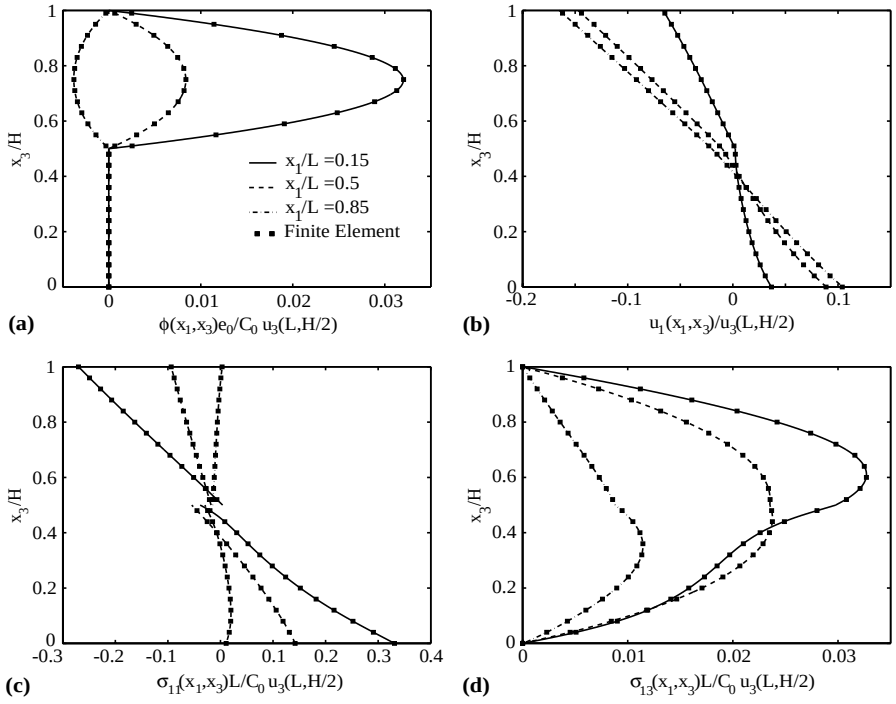

Fig. 4. Through-the-thickness variation of the electric potential, axial displacement, longitudinal stress and transverse shear stress for the cantilever graphite/epoxy-PZT5A composite plate compared to the finite element solution for mode 1.

to the peaks in the displacement vs. frequency curve. Natural frequencies corresponding to the higher axial modes of vibration can be obtained by applying a sinusoidal potential $\phi(x_1, H) = \phi_0 \sin(q\pi x_1/L)\cos\omega t$ to the top surface of the piezoelectric plate, where q is an integer that determines the axial mode.

Finite element (FE) analysis was also performed using ABAQUS (ABAQUS, 2002) for comparison. The FE solution is based on the plane strain assumption in which $u_3 = 0$ and u_1, u_2 and ϕ are functions of x_1, x_2 and t. The FE mesh consisted of 10,000 eight noded biquadratic elements. The first five thickness modes corresponding to the first axial mode of vibration obtained from our analytical solution are compared with those given by Heyliger and Brooks (1995) and the FE method in Table 2. The natural frequencies from the three solution procedures are nearly identical. The computational effort required to obtain the Fourier coefficients for the analytical solution is nearly the same as the effort required for the FE analysis. However, it should be noted that the analytical solution satisfies the equation of motion and charge equation exactly at every point within the body, whereas the FE solution satisfies these equations only in a weak sense. Furthermore, once a computer program has been developed to compute the Fourier coefficients, the input is essentially trivial and no discretization of the domain and no element connectivity is required.

5.2. Two-layer cantilever composite plate

Consider a two-ply piezoelectric composite laminate with the bottom layer made of graphite/epoxy with fibers parallel to the x_1-axis and the top layer made of PZT-5A. The dimensions of the composite plate are

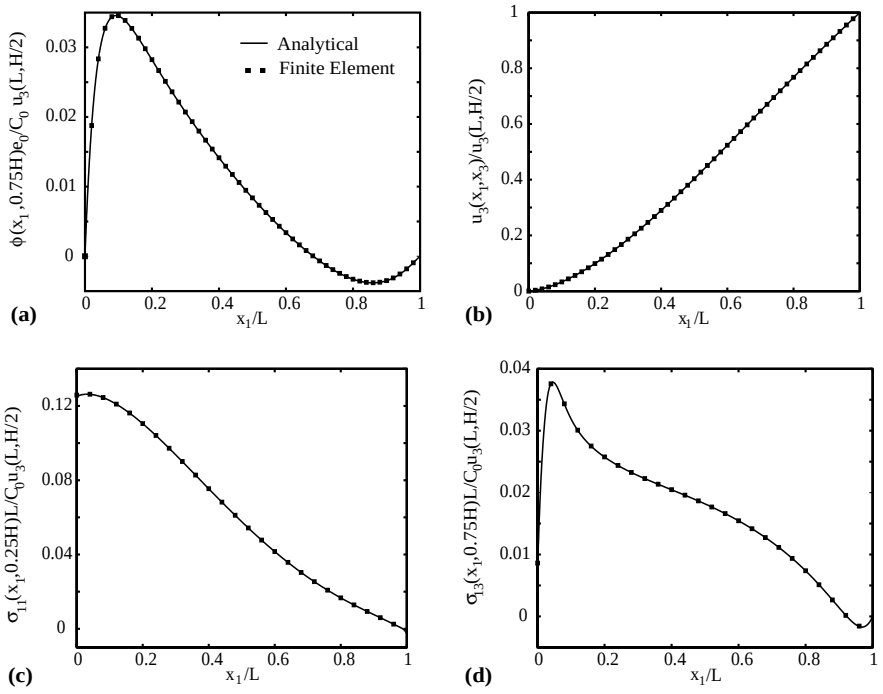

Fig. 5. Axial variation of the electric potential, transverse displacement, longitudinal stress and transverse shear stress for the cantilever graphite/epoxy-PZT5A composite plate compared to the finite element solution for mode 1.

$L = 0.1$ m, $H = 0.025$ and both layers are of equal thickness. The edge $x_1 = 0$ is clamped (i.e., $u_1 = u_2 = u_3 = 0$) and the edge $x_1 = L$ is traction free (i.e., $\sigma_{11} = \sigma_{12} = \sigma_{13} = 0$). The edges and top surface of the PZT-5A layer are electrically grounded to zero potential. The interface between the PZT-5A and graphite/epoxy layers is electroded and electrically grounded to zero potential.

The effect of truncation of the series on the accuracy of the natural frequencies, displacements and stresses corresponding to the first mode of vibration is investigated by computing the solution at specific points in the laminate. The first natural frequency and the corresponding displacements, electric potential and stresses at specific points of the piezoelectric composite laminate are listed in Table 3 for increasing number of terms K. The natural frequencies are normalized as $\bar{\omega}_j = \omega_j(L^2/H)\sqrt{\rho_0/C_0}$, $\rho_0 = 7750$ kg/m^3 and $C_0 = 99.201$ GPa. These results show that the natural frequencies, mechanical displacements, stresses and electric potential converge rapidly. The results in this section are computed using $K = 400$.

The first 12 mode shapes and the corresponding natural frequencies are shown in Fig. 3. The mode shapes are depicted by plotting the deformed shapes of material lines that in the reference configuration are parallel to the x_1- and x_3-axes. There is significant change in the thickness of the laminate for modes 9 and 12.

The through-the-thickness variation of the electric potential ϕ, axial displacement u_1, longitudinal stress σ_{11} and transverse shear stress σ_{13} at three locations along the span of the laminate for the first mode of vibration are shown in Fig. 4 along with values obtained from FE analysis (ABAQUS, 2002). Since displacements and stresses at a natural frequency are very large, they have been normalized by the value of the tip deflection, $u_3(L, H/2)$. The analytical and the FE values are almost identical. The electric potential ϕ in

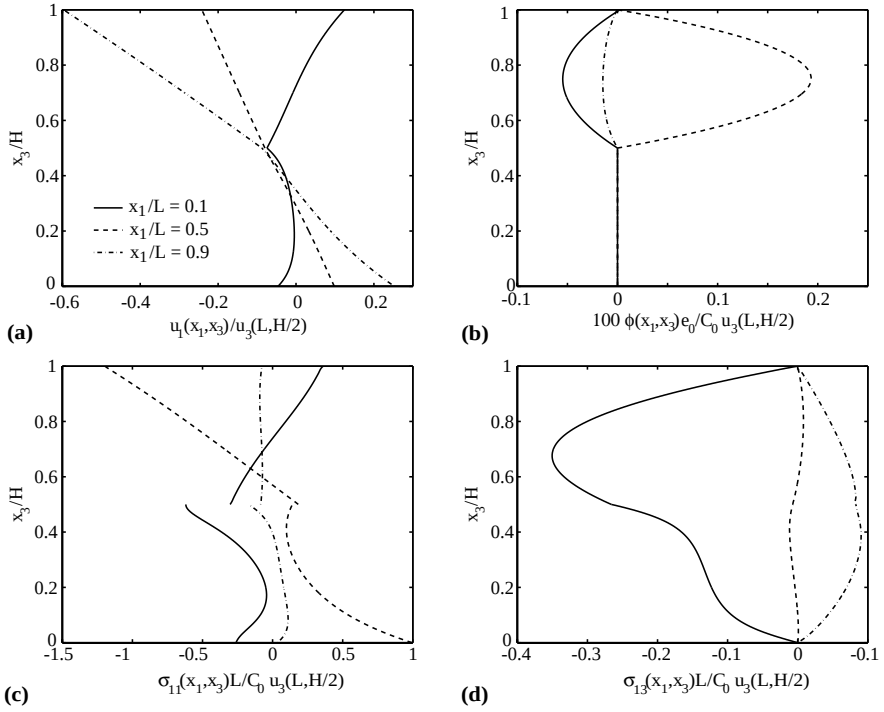

Fig. 6. Through-the-thickness variation of the axial displacement, electric potential, longitudinal stress and transverse shear stress for the cantilever graphite/epoxy-PZT5A composite plate for mode 2.

the piezoelectric layer has a parabolic variation in the thickness direction. The longitudinal stress σ_{11} is discontinuous at the interface $x_3/H = 0.5$ due to the discontinuity in the material properties of the two layers. The transverse shear stress σ_{13} is continuous across the interface between the layers since they are perfectly bonded together and tractions have been assumed to be continuous. Although the transverse shear stress σ_{13} is parabolic at the mid-span $x_1/L = 0.5$, it deviates from the parabolic profile near the clamped and free edges. The axial variations of the electric potential, transverse deflection, longitudinal stress and transverse shear stress are depicted in Fig. 5. A steep variation of the electric potential ϕ and of the transverse shear stress σ_{13} is observed at the clamped edge. Here too, the analytical and the FE results are in good agreement with each other.

The through-the-thickness distributions of the normalized axial displacement u_1, electric potential ϕ, longitudinal stress σ_{11} and transverse shear stress σ_{13} at four sections along the span of the cantilever laminate for the second mode of vibration are shown in Fig. 6. Although the axial displacement u_1 is an affine function of the thickness coordinate at the mid-span $x_1/L = 0.5$, it is non-linear near the clamped edge $x_1 = 0.1L$ and the free edge $x_1/L = 0.9$ (see Fig. 6a). It should be noted that the transverse shear stress does not have a parabolic profile in the thickness direction as is usually the case for a monolithic homogenous plate.

Fig. 7 exhibits the through-the-thickness variation of the axial displacement and stresses for the third mode of vibration. The axial displacements of all points in the thickness direction have the same sign, thus indicating that this is primarily an axial mode of vibration. The transverse shear stress σ_{13} is very large at the interface between the PZT-5A and the graphite/epoxy layers near the clamped and free edges of the

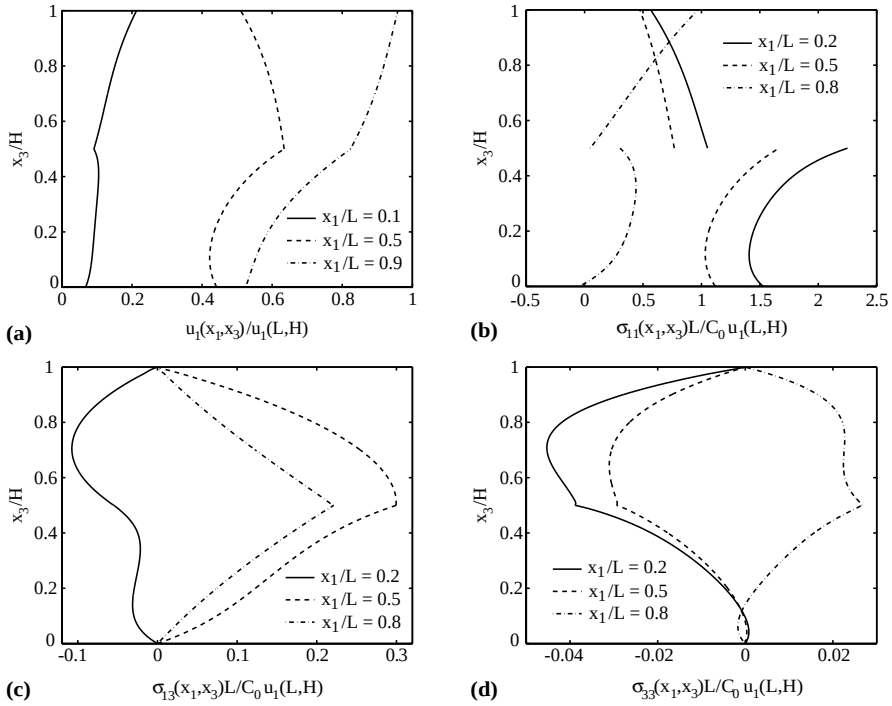

Fig. 7. Through-the-thickness variation of the axial displacement, electric potential, longitudinal stress and transverse shear stress for the cantilever graphite/epoxy-PZT5A composite plate for mode 3.

plate. The transverse normal stress σ_{33} is depicted in Fig. 7d. The longitudinal stress σ_{11} is an order of magnitude larger than the transverse shear stress σ_{13}, which in turn is an order of magnitude larger than the transverse normal stress σ_{33}.

It should be noted that the stresses and electric displacement field could be singular at points where the top surface, bottom surface and interfaces intersect the edges. The asymptotic solution at these points can be analyzed by assuming that the displacement and electric potential to be proportional to $z_\alpha^{\delta+1}$, where $z_\alpha = x_1 + q_\alpha x_3$ and (x_1, x_3) is measured from the point and δ is an eigenvalue to be determined (Ting, 1996). In our analysis, we have not explicitly included terms to represent the singular stress fields.

5.3. Cantilever plate with surface-boded piezoelectric segmented actuator

The final example concerns a homogeneous graphite/epoxy cantilever substrate with a PZT-5A actuator patch bonded to its upper surface as shown in Fig. 8. The dimensions are $L = 0.1$ m and $H = 0.25$ m. The

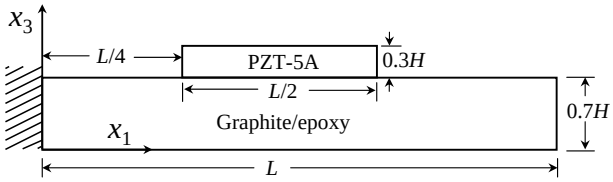

Fig. 8. Cantilever graphite/epoxy substrate with a segmented PZT-5A actuator bonded to its upper surface.

faces $x_3 = 0.7H$ and H of the PZT actuator are electroded and electrically grounded and the edges $x_1 = 0.25L$ and $0.75L$ are free of electric charge ($D_1 = 0$). To accommodate the abrupt change in thickness of the structure due to the piezoelectric actuator, we divide the graphite/epoxy substrate into three regions by introducing virtual vertical interfaces at $x_1 = L/4$ and $3L/4$. The continuity of the mechanical displacements and tractions are enforced along these vertical interfaces. Due to the introduction of the vertical interfaces, the structure consists of four laminae including the actuator. The first six natural frequencies and mode shapes are depicted in Fig. 9. Unlike the other five modes of vibration, there is significant axial extension of the beam in the fourth mode of vibration.

Through-the-thickness variations of the longitudinal stress σ_{11} at three locations along the span of the beam for the first four modes are shown in Fig. 10. The variation of the longitudinal stress in almost affine at $x_1 = 0.2L$ in the first mode of vibration as shown in Fig. 10a. However, the through-the-thickness variation of σ_{11} is non-linear at the location $x_1 = 0.26L$ which is close to the edge of the PZT actuator, and is highly non-linear for the higher modes of vibration. The through-the-thickness variations of the transverse shear stress σ_{13} for the first four modes of vibration are given in Fig. 11. It is observed that the transverse shear stress is very large at the edge of the PZT/substrate interface, as depicted by plots of σ_{13} vs. x_3 at $x_1 = 0.26L$. The shear stresses are singular at the corners $(0.25L, 0.7H)$ and $(0.75L, 0.7H)$ at the interface between the piezoelectric actuator and the graphite/epoxy substrate. These corners, when viewed asymptotically, are special points where a PZT wedge comes in contact with a graphite–epoxy surface. The mismatch in the material properties causes stress singularity at these points (Vel and Batra, 2000b).

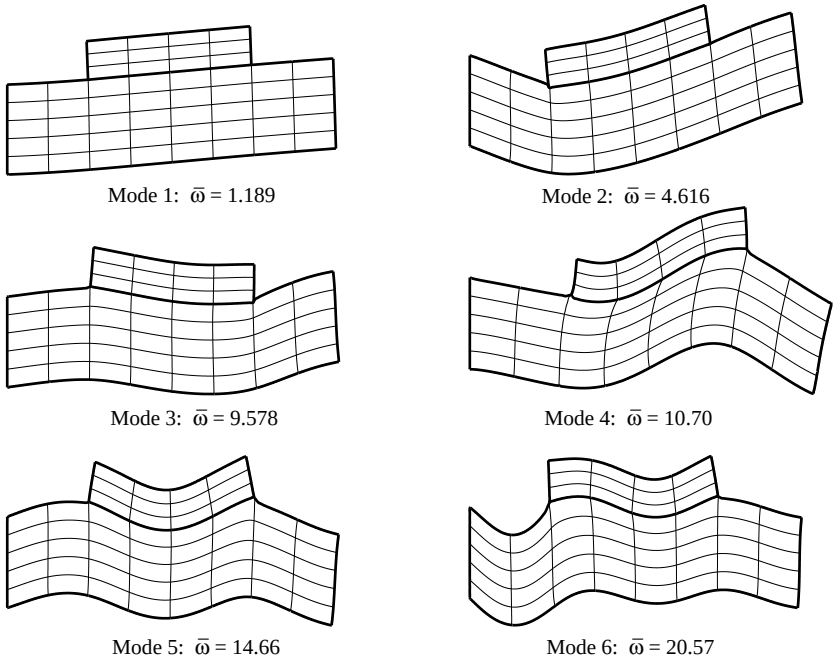

Fig. 9. The first six normalized natural frequencies and mode shapes for the graphite/epoxy cantilever plate with segmented actuator.

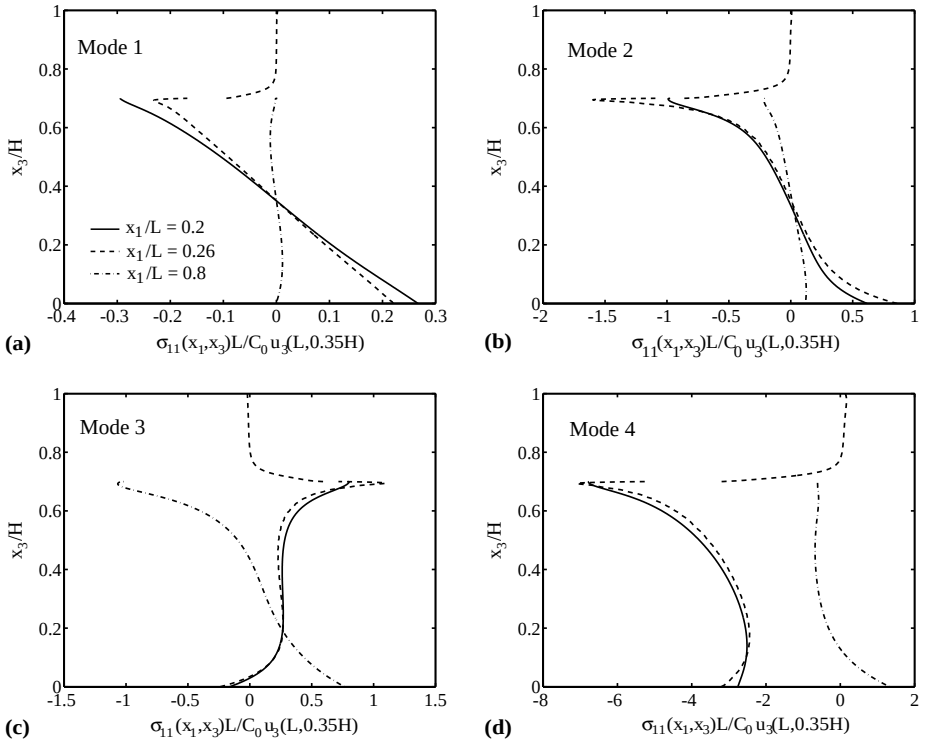

Fig. 10. Through-the-thickness variation of the longitudinal stress for the first four modes of the graphite/epoxy cantilever plate with segmented actuator.

6. Conclusions

We have extended the Stroh formalism to obtain an analytical solution for the steady state vibration of a composite plate with either surface mounted or embedded piezoelectric patches. Fourier basis functions for the mechanical displacements and electric potential that identically satisfy the equations of motion and charge equation of electrostatics are used to solve the boundary value problem via the superposition principle. The boundary conditions at the edges and continuity conditions at interfaces between adjoining laminae are satisfied in the sense of Fourier series. The mechanical displacements, electric potential, stresses and electric displacement can be computed to a desired degree of accuracy by retaining sufficiently large number of terms in the series solution.

The solution procedure is validated by comparing the natural frequencies of a simply supported thick piezoelectric plate with those given by Heyliger and Brooks (1995). We have computed the first 12 natural frequencies and mode shapes for a two-layer graphite/epoxy-PZT cantilever composite plate. The analytical displacements, stresses and electric potential compare very well with those obtained by the finite element method. We have also analyzed the natural frequencies, mode shapes, displacements and stresses for a cantilever graphite/epoxy lamina with a segmented PZT actuator on it top surface. The transverse shear stress is very large at the edges of the PZT-substrate interface. As illustrated by the results, the method is versatile and capable of analyzing piezoelectric composite plates subjected to arbitrary boundary conditions at the edges.

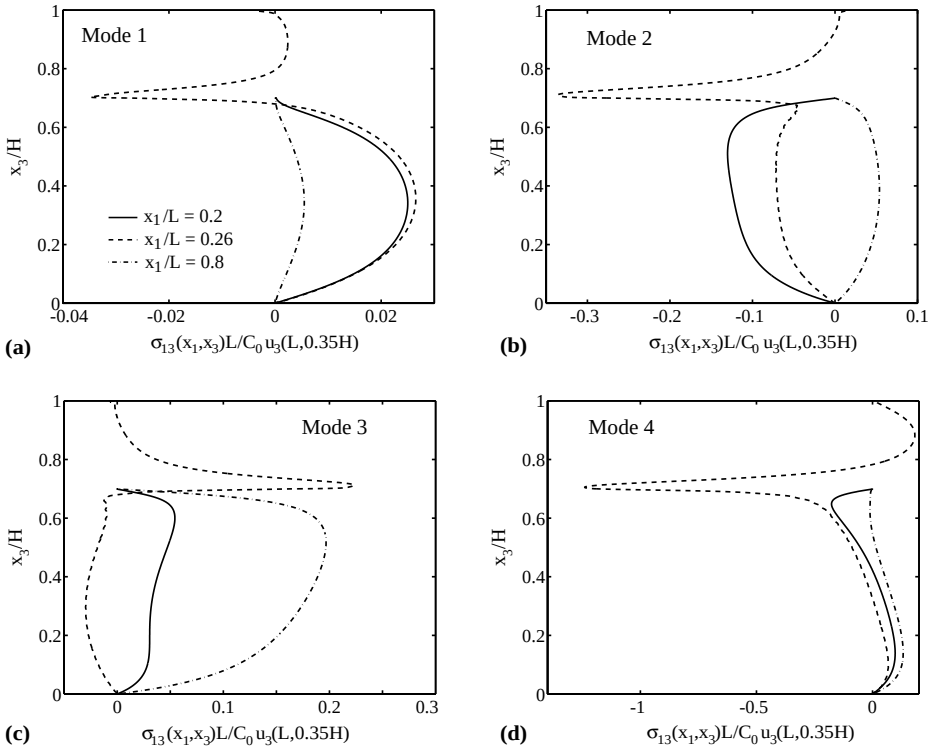

Fig. 11. Through-the-thickness variation of the transverse shear stress for the first four modes of the graphite/epoxy cantilever plate with segmented actuator.

References

ABAQUS Users Manual, 2002. Version 6.3, Hibbit, Karlsson & Sorensen, Inc.

Allik, H., Hughes, T.J.R., 1970. Finite element method for piezoelectric vibration. International Journal for Numerical Methods in Engineering 2, 151–157.

Bailey, T., Hubbard, J.E., 1985. Distributed piezoelectric-polymer active vibration control of a cantilever beam. Journal of Guidance, Control, and Dynamics 8, 605–611.

Batra, R.C., Aimmanee, S., 2003. Missing frequencies in previous exact solutions of free vibrations of simply supported rectangular plates. Journal of Sound and Vibrations 265, 887–896.

Batra, R.C., Geng, T.S., 2002. Comparison of active constrained layer damping by using extension and shear mode actuators. Journal of Intelligent Material Systems and Structures 12.

Batra, R.C., Ghosh, K., 1995. Deflection control during dynamic deformations of a rectangular plate using piezoceramic elements. AIAA Journal 33, 1547–1548.

Batra, R.C., Liang, X.Q., 1997a. The vibration of a rectangular laminated elastic plate with embedded piezoelectric sensors and actuators. Computers and Structures 63, 203–216.

Batra, R.C., Liang, X.Q., 1997b. Finite dynamic deformations of smart structures. Computational Mechanics 20, 427–438.

Batra, R.C., Liang, X.Q., Yang, J.S., 1996a. The vibration of a simply supported rectangular elastic plate due to piezoelectric actuators. International Journal of Solids and Structures 33, 1597–1618.

Batra, R.C., Liang, X.Q., Yang, J.S., 1996b. Shape control of vibrating simply supported rectangular plates. AIAA Journal 34, 116–122.

Bisegna, P., Maceri, F., 1996. An exact three-dimensional solution for simply supported rectangular piezoelectric plates. Journal of Applied Mechanics 63, 628–638.

Brooks, S., Heyliger, P., 1994. Static behavior of piezoelectric laminates with distributed and patched actuators. Journal of Intelligent Material Systems and Structures 5, 635–646.

Crawley, E.F., Anderson, E.H., 1990. Detailed models of piezoceramic actuation of beams. Journal of Intelligent Material Systems and Structures 1, 4–25.

Crawley, E.F., de Luis, J., 1987. Use of piezoelectric actuators as elements of intelligent structures. AIAA Journal 25, 1373–1385.

Eshelby, J.D., Read, W.T., Shockley, W., 1953. Anisotropic elasticity with applications to dislocation theory. Acta Metallurgica 1, 251–259.

Ghosh, K., Batra, R.C., 1995. Shape control of plates using piezoceramic elements. AIAA Journal 33, 1354–1357.

Ha, S.K., Keilers, C., Chang, F.K., 1992. Finite element analysis of composite structures containing piezoceramic sensors and actuators. AIAA Journal 30, 772–780.

Heyliger, P., 1994. Static behavior of laminated elastic/piezoelectric plates. AIAA Journal 32, 2481–2484.

Heyliger, P., 1997. Exact solutions for simply supported laminated piezoelectric plates. Journal of Applied Mechanics 64, 299–306.

Heyliger, P., Brooks, S., 1995. Free vibration of piezoelectric laminates in cylindrical bending. International Journal of Solids and Structures 32, 2945–2960.

Heyliger, P., Brooks, S., 1996. Exact solutions for laminated piezoelectric plates in cylindrical bending. Journal of Applied Mechanics 63, 903–910.

Heyliger, P., Saravanos, D.A., 1995. Exact free-vibration analysis of laminated plates with embedded piezoelectric layers. Journal of the Acoustical Society of America 98, 1547–1555.

Lee, C.K., 1990. Theory of laminated piezoelectric plates for the design of distributed sensors/actuators. part 1: governing equations and reciprocal relationships. Journal of the Acoustic Society of America 87, 1144–1158.

Lee, J.S., Jiang, L.Z., 1996. Exact electroelastic analysis of piezoelectric laminae via state space approach. International Journal of Solids and Structures 33, 977–990.

Mitchell, J.A., Reddy, J.N., 1995. A refined hybrid plate theory for composite laminates with piezoelectric laminae. International Journal of Solids and Structures 32, 2345–2367.

Robbins, D.H., Reddy, J.N., 1991. Analysis of piezoelectrically actuated beams using a layer-wise displacement theory. Computers and Structures 41, 265–279.

Stroh, A.N., 1958. Dislocations and cracks in anisotropic elasticity. Philosophical Magazine 3, 625–646.

Tiersten, H.F., 1969. Linear piezoelectric plate vibrations. Plenum Press, New York.

Ting, T.C.T., 1996. Anisotropic Elasticity. Theory and Applications. In: Oxford Engineering Science Series, vol. 45. Oxford Univ Press, New York.

Vel, S.S., Batra, R.C., 2000a. Three-dimensional analytical solution for hybrid multilayered piezoelectric plates. Journal of Applied Mechanics 67, 558–567.

Vel, S.S., Batra, R.C., 2000b. Cylindrical bending of laminated plates with distributed and segmented piezoelectric actuators/sensors. AIAA Journal 38, 857–867.

Vel, S.S., Batra, R.C., 2001a. Exact solution for the cylindrical bending of laminated plates with embedded shear actuators. Smart Materials and Structures 10, 240–251.

Vel, S.S., Batra, R.C., 2001b. Exact solution for rectangular sandwich plates with embedded piezoelectric shear actuators. AIAA Journal 39, 1363–1373.

Vel, S.S., Batra, R.C., 2002. Exact solutions for thermoelastic deformations of functionally graded thick rectangular plates. AIAA Journal 40 (7), 1421–1433.

Vel, S.S., Batra, R.C., 2003. Exact thermoelasticity solution for cylindrical bending vibrations of functionally graded plates. In: Watanabe, K., Ziegler, F. (Eds.), Proc. IUTAM Symp. on Dynamics of Advanced Materials and Smart Structures. Kluwer Academic Publishers, Dordrecht, Boston, London, pp. 429–438.

Wang, B.T., Rogers, C.A., 1991. Laminate plate theory for spatially distributed induced strain actuators. Journal of Composite Materials 25, 433–452.

Yang, J.S., Batra, R.C., Liang, X.Q., 1994. The cylindrical bending vibrations of a laminated elastic plate due to piezoelectric actuators. Smart Materials and Structures 3, 485–493.